DOI: 10.1002/anie.201200244

Arresting Particle Growth

Structural and Mechanistic Revelations on an Iron Conversion Reaction from Pair Distribution Function Analysis**

Badri Shyam, Karena W. Chapman, Mahalingam Balasubramanian, Robert J. Klingler, George Srajer, and Peter J. Chupas*

In the development of high-performance energy conversion and storage systems, understanding the atomic structure of nanomaterials is of increasing relevance.[1] In the case of chemical energy storage, conversion chemistries promise capacities many times those of existing insertion-based Li ion batteries—a consequence of the multiple, rather than single, electron reaction at each metal atom.[2] In the conversion process, metal compounds (e.g., oxides, fluorides, etc.) react with Li to produce metal and Li salts (e.g., Li_2O, LiF), undergoing extensive chemical and structural rearrangement.[3,4] In such reactions, nanomaterials are not only associated with enhanced reversibility (i.e. cyclability), but the electrode particles often reduce further in size during discharge (electrochemical grinding).[1,4] Conventional crystallographic probes offer limited insight into these nanomaterials and reactions,[5] and thus, with a tremendous gain in capacity comes increased challenges, in both understanding and optimizing this process. Typically, reaction products and intermediates are only identified tentatively, by matching poorly defined features in the diffraction data to known structures. The most in depth understanding of the conversion process to date, has been gained by combining insights from many different characterization tools, including diffraction, X-ray absorption spectroscopies, NMR spectroscopy, and TEM imaging.[6]

Here we show that systematic application of pair distribution function (PDF) analysis alone, can yield comprehensive insight into conversion processes, including key mechanistic and structural details. This is demonstrated for nanoscale α-Fe_2O_3, a prototypical example of a conversion material.[7–9] The PDF method has emerged as a valuable probe of nanomaterial structure, providing insights from the immediate coordination environment extending to several nm, towards the length scale of a nanoparticle.[10] Accordingly, the method allows reliable identification of phases, detailed structural insights, evaluation of changes in particle dimensions, and quantitative determination of phase fractions throughout a reaction.[11] For nanoscale α-Fe_2O_3, we identify significant deviations of the reaction products from bulk crystalline analogues, including local distortions, defects, and non-stoichiometries. The structure of a key reaction intermediate is clearly elucidated for the first time. The metal nanoparticles produced by the reaction are found to be not simply small particles of α-Fe, as previously presumed, but are rich in defects and, contrary to expectation, do not grow or agglomerate. These characteristics—a proposed defect-inhibited particle growth—may hold the key to the reversibility of the conversion reaction in this system.

α-Fe_2O_3 (hematite) is part of a broad family of promising high capacity, conversion-based electrode materials, with the added advantage of iron being amongst the most abundant terrestrial elements, with minimal health or environmental impacts.[3,6–9,12] Efforts to develop nanostructured α-Fe_2O_3 have produced amongst the highest reversible capacities for iron-based electrodes.[9] Nanoscale α-Fe_2O_3 (60–200 Å diameter) was prepared by the forced acid hydrolysis of iron nitrate in water at 100 °C.[8] A composite electrode film of α-Fe_2O_3 and carbon was cycled against Li metal in a coin cell. The potential decreases steeply up to 2 Li, flattening slightly between 2 and 1.5 V, then plateaus at 0.8 V between 2 and 6 Li—a capacity of 1002 mA h g^{-1} for 6 Li (Figure 1).[13] The reaction proceeded beyond 6 Li per 2 Fe^{3+}, up to 8 Li, with this excess capacity ascribed to electrolyte decomposition.[8]

Total scattering data were collected for electrodes recovered from intermediate states of discharge corresponding to 0–8 Li per Fe_2O_3. The high-energy X-rays ($\lambda = 0.2128$ Å) available at beamline 11-ID-B at the Advanced Photon Source at Argonne National Laboratory were used to collect data to high values of momentum transfer ($Q_{max} = 24$ Å^{-1}).[14] The PDFs, $G(r)$, contain peaks corresponding to the atom–atom distances within the sample weighted by the scattering power of the atoms involved.

The PDFs indicate that the discharge reaction proceeds through two distinct transitions each accompanied by a reduction in particle size (Figure 1a). Models were fit to the data within PDFgui,[15] using a "real space Rietveld" approach, to assess the atomic structure and phase distribution. The initial hexagonal α-Fe_2O_3 electrode ($R\bar{3}c$, $a = 5.0267(5)$ Å, $c = 13.7301(2)$ Å) forms a cubic rock salt phase ($Fm\bar{3}m$, $a = 4.2035$ Å, 50–60 Å diameter) near 2 Li; this transforms to

[*] Dr. B. Shyam, Dr. K. W. Chapman, Dr. M. Balasubramanian, Dr. R. J. Klingler, Dr. G. Srajer, Dr. P. J. Chupas
X-ray Science Division, Advanced Photon Source
Argonne National Laboratory
9700 South Cass Avenue, Argonne, IL 60439 (USA)
E-mail: chapmank@aps.anl.gov

[**] Work done at Argonne and use of the Advanced Photon Source (APS), an Office of Science User Facility operated for the U.S. DOE Office of Science by Argonne National Laboratory, were supported by the U.S. DOE under Contract No. DE-AC02-06CH11357. The electrochemistry laboratory maintained by the Structural Science group at the APS is jointly supported by Argonne and the Northeastern Center for Chemical Energy Storage, an Energy Frontier Research Center funded by the U.S. DOE under award No. DE-SC0001294. We acknowledge discussions with K. Wiaderek, S. Pol, O. Borkiewicz, R. Winans, K. Nemeth, S. Heald, and G. Sandi-Tapia.

Supporting information for this article is available on the WWW under http://dx.doi.org/10.1002/anie.201200244.

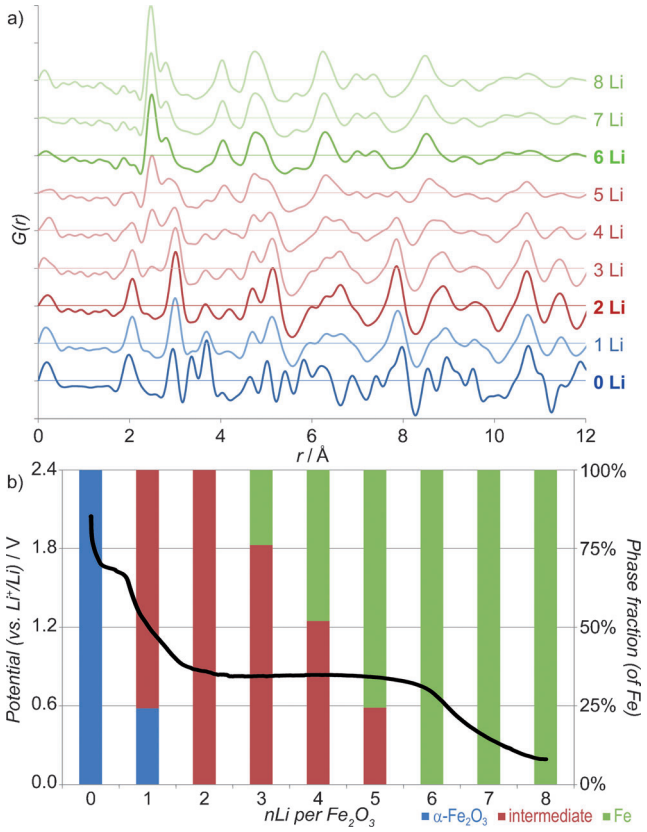

Figure 1. a) The PDFs, $G(r)$, obtained during the electrochemical reaction of α-Fe_2O_3 with Li. The pure phases formed near 0, 2, and 6 Li are in bold. b) The distribution of Fe from quantitative fits to the PDF data. The corresponding galvanostatic curve is overlaid.

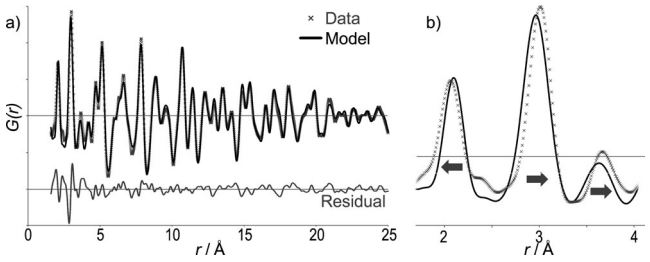

Figure 2. a) A fit of a rock salt model to the PDF at 2 Li ($R_{4\text{-}25Å}$=15.1 %), highlighting b) the distortions of the local structure.

Fe nanoparticles with a body-centered cubic-like structure (bcc, $a = 2.9$ Å, 18 Å diameter) by 6 Li.

This phase analysis is ostensibly consistent with the phases reported in earlier crystallographic studies,[7,8] however, the present PDF analysis yields new insights, of unprecedented detail, into how the atomic structure of the reaction products deviate from the crystallographic models. This includes non-stoichiometries, local distortions, and defects of the intermediate "rock salt" phase and final metal nanoparticles.

Although the intermediate that exists near 2 Li classifies as a rock salt phase, with an alternating cubic lattice of cations (Fe) and anions (O^{2-}), this structure type encompasses several proposed Li–Fe–O phases with distinct stoichiometries, Li distributions and defects.[8,16] A rock salt model provided an excellent fit to the PDF data beyond 4 Å (Figure 2), with local distortions evident as deviations in the positions of first three peaks ($d_{Fe\text{-}O}$, $d_{Fe\cdots Fe}$, $d_{Fe\cdots O}$). Similar structural parameters and local distortions were obtained for a rock salt phase produced by chemical lithiation of α-Fe_2O_3 (see Supporting Information). Fits of Gaussian functions to these peaks indicate that the Fe–O bond length is contracted to 2.062 Å (cf. 2.102 Å $= a/2$), and the Fe···Fe and Fe···O distances are expanded to 3.002 Å and 3.683 Å, respectively (*cf.* 2.973 Å $= a/\sqrt{2}$ and 3.641 Å $= a\sqrt{3}/2$), relative to the crystallographic model where atoms are constrained to special positions.

While the data are poorly sensitive to the position and occupancy of Li within the structure, refinement of Fe and O occupancies indicates a depletion of oxygen compared to the initial material. The refined Fe:O ratio was in the range 0.8–0.95:1 with the value depending on the *r*-range used in the fit. There are two important implications of this Fe:O stoichiometry. Firstly, that a second oxide (e.g., Li_2O) forms during the transition to this intermediate, although this extra phase is not apparent in the X-ray PDF data which is dominated by strongly scattering Fe phases. Secondly, that the implied Fe oxidation state is greater than 2 (2.1–2.5), although this estimate does not reflect any lithium that may be within the lattice or any under-coordination of Fe ions at the particle surface.[17] The Fe–O bondlength is consistent with an intermediate average Fe oxidation state, being between those typical of Fe^{2+}–O and Fe^{3+}–O, and with an oxidation state of 2.45 indicated from a bond valence sum calculation.

The Fe:O ratio matches that of wüstites—$Fe_{1-x}O$ for x up to 0.15. Wüstite is a mixed valence (Fe^{2+}/Fe^{3+}) rock salt phase with complex defect structures involving correlated octahedral cation vacancies (Fe^{2+}) and interstitial cations (Fe^{3+}) in tetrahedral sites.[18] The local structure distortions present in wüstite are precisely consistent with those observed in the rock salt intermediate (see Supporting Information). While formation of wüstite in this reaction was dismissed in previous crystallographic studies[7,8] based on its slightly larger lattice parameter (4.3 Å), incorporation of Li in a wüstite structure, for example through substitution of these smaller cations at the tetrahedral interstices, could reduce the lattice dimensions. Accordingly, we propose that the atomic structure of the rock salt intermediate is related to that of wüstite, possibly including octahedral Fe vacancies, mixed valency, and Li cations in the tetrahedral interstices. The rich chemistries of wüstite-type phases (including redox-buffer phenomena and solid solution behavior)[18] could play an important role in the electrochemical properties of this system.

The PDFs corresponding to the Fe nanoparticles were isolated from the multi-phase data by subtracting the scaled rock salt contribution (Figure 3). While the nanoparticles that form as the reaction progresses are of consistent diameter (ca. 18 Å, ca. 250 atoms), their atomic structure is dynamic and evolves continuously with lithiation. The PDFs of the nanoparticles deviate from the ideal bcc α-Fe structure: peak splitting at high r suggests distortion from cubic symmetry; the intensity of peaks at 4 and 4.8 Å are under- and overestimated, respectively; the feature at 2.8 Å that reflects

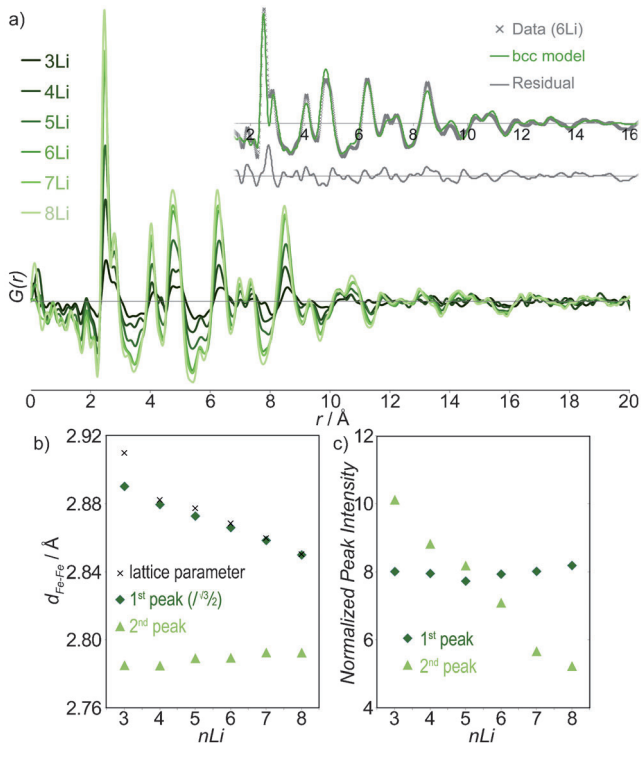

Figure 3. a) The evolving PDFs of the Fe nanoparticles. A representative fit of a α-Fe (bcc) model to the data is inset. b) The evolution of the Fe–Fe distances. c) Fe–Fe peak intensities.

the second Fe···Fe distance, is contracted with greater intensity than expected based on the 8:6 ratio of first to second coordination shells in body-centered packing. The nanoparticle structure refines, becoming more bcc-like with increased lithiation—although not perfectly so. Features in the PDF sharpen and split peaks coalesce. The average lattice dimensions contract, from unexpectedly larger than bulk Fe to less than bulk Fe as is typical of nanoparticles.[19] The nearest Fe–Fe distance (2.5 Å) contracts commensurate with the lattice parameter, and increases intensity proportionately with the total nanoparticle signal. In contrast, the second Fe···Fe distance is relatively invariant (expands slightly), and its relative intensity decreases such that the ratio of peak intensities approaches 8:6. These changes in nanoparticle structure occur continuously, including in the region beyond 6 Li where no extra Fe is generated. A weak non-bcc feature evident in the data, at ca. 1.88 Å, initially grows then decreases in intensity (a continuous decrease relative to the total nanoparticle signal). This feature may correspond to Fe–O correlations in four-coordinate Fe^{3+} species, O···O correlations in CO_3^{2-} anions within the solid-electrolyte interface or coordinated at the particle surface, or trapped interstitial species.

The atomic distances and coordination numbers available from the position and intensity of peaks in the PDF provide direct insight into the nature of defects within the nanoparticles and how they deviate from the ideal bcc model. The first Fe–Fe peak, at 2.5 Å, mirrors the global changes to the nanoparticle. By contrast, the second Fe–Fe feature evolves differently, with consistently shorter average distance and with intensity only approaching expected values (8:6 ratio) upon completion of the lithiation reaction. Residual intensity in fits of the α-Fe model, at 2.66 Å, close to the atom–atom distance for close-packed first-row transition metals, suggests that the excess intensity may be associated with close-packed defects, either within the nanoparticle or at the particle surface. Such defects may contribute to the distortions of the nanoparticle, and the greater lattice dimensions relative to bulk α-Fe. A decreasing concentration of these defects with increasing lithiation, may underlie the increasing bcc character of the structure and the contraction of lattice dimensions.

For α-Fe_2O_3, the initially nanoscale electrode particles are further reduced in size with each phase transition during electrochemical lithiation. Not only can this evolution in particle dimensions be quantified in the PDFs analysis, but the direct insight into the atomic structures illuminates several key mechanistic points.

1) The Fe nanoparticles formed are of constant size, without significant growth throughout the discharge process. High atom mobility is typical of such small metal particles and, accordingly, particle growth and coarsening is often observed. In the present system, particle growth is likely inhibited through surface passivation or through strain-inhibited or defect frustrated growth. The reversibility of conversion reactions relies on being able to recombine multiple discharge products to recover the original phase. The nanoscale characteristic of the discharge product, overcomes limitations associated with atom diffusion and recombination, thus, aiding reversibility.

2) The structure of the "rock salt" intermediate, including its stoichiometry and local defects, have been quantified for the first time. This phase shares characteristics of wüstite,[20] with an Fe:O ratio approaching 1:1. It is deficient in oxygen compared to the initial material as well as the previously suggested intermediate formulas ($Li_2Fe_2O_3$ or α-$LiFeO_2$ cubic "rock salt" phases) tentatively identified based on only a handful of Bragg peaks.[7,8] The defect structure of this rock salt intermediate may be key to forming the defective Fe nanoparticles and similar intermediates are likely in related conversion materials.

In summary, we demonstrate that PDF analysis can provide a comprehensive understanding of the complex reactions characteristic of electrochemical conversion. This level of insight could only be otherwise obtained by combining many different characterization tools and, as such, the PDF methodology has a promising role in the rational development of nanomaterials for energy conversion and storage.[1,21] The frustrated nanoparticle growth observed here is not only relevant to reversible electrochemical energy storage but is of fundamental interest in catalysis, where activity is strongly linked to particle size and defect concentration. We anticipate that by targeting defective metal particles, for example, through chemical doping, it will be possible to induce strain and inhibit particle growth in the discharged materials and, hence, improve cyclability—a critical performance limitation in higher capacity conversion electrodes.

Received: January 10, 2012
Published online: April 11, 2012

Keywords: electrochemistry · energy conversion · iron · nanoparticles · pair distribution function (PDF)

[1] a) A. S. Aricò, P. Bruce, B. Scrosati, J. M. Tarascon, W. Van Schalkwijk, *Nat. Mater.* **2005**, *4*, 366; b) P. G. Bruce, B. Scrosati, J. M. Tarascon, *Angew. Chem.* **2008**, *120*, 2972; *Angew. Chem. Int. Ed.* **2008**, *47*, 2930; c) K. T. Lee, J. Cho, *Nano Today* **2011**, *6*, 28.

[2] P. Poizot, S. Laruelle, S. Grugeon, L. Dupont, J. M. Tarascon, *Nature* **2000**, *407*, 496.

[3] J. Cabana, L. Monconduit, D. Larcher, M. R. Palacin, *Adv. Mater.* **2010**, *22*, E170.

[4] a) D. Deng, J. Y. Lee, *Angew. Chem.* **2009**, *121*, 1688; *Angew. Chem. Int. Ed.* **2009**, *48*, 1660; b) Y. Yu, L. Gu, C. B. Zhu, P. A. van Aken, J. Maier, *J. Am. Chem. Soc.* **2009**, *131*, 15984; c) H. Kim, M. Seo, M. H. Park, J. Cho, *Angew. Chem.* **2010**, *122*, 2192; *Angew. Chem. Int. Ed.* **2010**, *49*, 2146; d) J. S. Chen, Y. L. Tan, C. M. Li, Y. L. Cheah, D. Y. Luan, S. Madhavi, F. Y. C. Boey, L. A. Archer, X. W. Lou, *J. Am. Chem. Soc.* **2010**, *132*, 6124; e) Y. Ren, A. R. Armstrong, F. Jiao, P. G. Bruce, *J. Am. Chem. Soc.* **2010**, *132*, 996; f) D. Dambournet, K. W. Chapman, P. J. Chupas, R. E. Gerald, N. Penin, C. Labrugere, A. Demourgues, A. Tressaud, K. Amine, *J. Am. Chem. Soc.* **2011**, *133*, 13240; g) J. F. Ye, W. Liu, J. G. Cai, S. A. Chen, X. W. Zhao, H. H. Zhou, L. M. Qi, *J. Am. Chem. Soc.* **2011**, *133*, 933.

[5] S. J. L. Billinge, I. Levin, *Science* **2007**, *316*, 561.

[6] a) N. Yamakawa, M. Jiang, B. Key, C. P. Grey, *J. Am. Chem. Soc.* **2009**, *131*, 10525; b) F. Wang, R. Robert, N. A. Chernova, N. Pereira, F. Omenya, F. Badway, X. Hua, M. Ruotolo, R. Zhang, L. Wu, V. Volkov, D. Su, B. Key, M. S. Whittingham, C. P. Grey, G. G. Amatucci, Y. Zhu, J. Graetz, *J. Am. Chem. Soc.* **2011**, *133*, 18828.

[7] a) M. M. Thackeray, W. I. F. David, J. B. Goodenough, *Mater. Res. Bull.* **1982**, *17*, 785; b) M. M. Thackeray, W. I. F. David, J. B. Goodenough, *J. Solid State Chem.* **1984**, *55*, 280.

[8] a) D. Larcher, C. Masquelier, D. Bonnin, Y. Chabre, V. Masson, J. B. Leriche, J. M. Tarascon, *J. Electrochem. Soc.* **2003**, *150*, A133; b) D. Larcher, D. Bonnin, R. Cortes, I. Rivals, L. Personnaz, J. M. Tarascon, *J. Electrochem. Soc.* **2003**, *150*, A1643.

[9] a) J. S. Chen, T. Zhu, X. H. Yang, H. G. Yang, X. W. Lou, *J. Am. Chem. Soc.* **2010**, *132*, 13162; b) B. Wang, J. S. Chen, H. B. Wu, Z. Wang, X. W. Lou, *J. Am. Chem. Soc.* **2011**, *133*, 17146.

[10] T. Egami, S. J. L. Billinge, *Underneath the Bragg Peaks: Structure Analysis of Complex Materials*, (Ed.: R. Cahn), Oxford/Pergamon, New York, **2004**.

[11] a) P. J. Chupas, K. W. Chapman, G. Jennings, P. L. Lee, C. P. Grey, *J. Am. Chem. Soc.* **2007**, *129*, 13822; b) H. Zhao, T. M. Nenoff, G. Jennings, P. J. Chupas, K. W. Chapman, *J. Phys. Chem. Lett.* **2011**, *2*, 2742.

[12] a) F. Badway, N. Pereira, F. Cosandey, G. G. Amatucci, *J. Electrochem. Soc.* **2003**, *150*, A1209; b) N. Pereira, F. Badway, M. Wartelsky, S. Gunn, G. G. Amatucci, *J. Electrochem. Soc.* **2009**, *156*, A407.

[13] Here "*n*" Li is used to refer to the number of Li atoms reacted per Fe_2O_3 formula unit in the composite electrode.

[14] P. J. Chupas, K. W. Chapman, P. L. Lee, *J. Appl. Crystallogr.* **2007**, *40*, 463.

[15] C. L. Farrow, P. Juhás, J. W. Liu, D. Bryndin, E. S. Božin, J. Bloch, T. Proffen, S. J. L. Billinge, *J. Phys. Condens. Matter* **2007**, *19*, 335219.

[16] a) N. A. Godshall, I. D. Raistrick, R. A. Huggins, *Mater. Res. Bull.* **1980**, *15*, 561; b) L. A. de Picciotto, M. M. Thackeray, *Mater. Res. Bull.* **1986**, *21*, 583.

[17] a) G. Jain, M. Balasubramanian, J. J. Xu, *Chem. Mater.* **2006**, *18*, 423; b) L. X. Chen, T. Liu, M. C. Thurnauer, R. Csencsits, T. Rajh, *J. Phys. Chem. B* **2002**, *106*, 8539.

[18] R. M. Hazen, R. Jeanloz, *Rev. Geophys.* **1984**, *22*, 37.

[19] J. T. Miller, A. J. Kropf, Y. Zha, J. R. Regalbuto, L. Delannoy, C. Louis, E. Bus, J. A. van Bokhoven, *J. Catal.* **2006**, *240*, 222.

[20] We note that the phase transitions upon electrochemical reduction of α-Fe_2O_3 with lithium parallels that observed on chemical reduction, for example, during ore refining (hematite–magnetite–wüstite–iron). During the lithiation reaction, magnetite formation is suppressed, with lithium insertion into the rock salt lattice potentially allowing a broader range of stoichiometries or valence states to be accommodated.

[21] D. K. Zhong, J. W. Sun, H. Inumaru, D. R. Gamelin, *J. Am. Chem. Soc.* **2009**, *131*, 6086.

